

Classification of ordering kinetics in three-phase systems

R. M. L. Evans, W. C. K. Poon, and F. Renth

Department of Physics and Astronomy, University of Edinburgh, Mayfield Road, Edinburgh EH9 3JZ, Scotland, United Kingdom

(Received 26 March 2001; published 30 August 2001)

Though equations of motion containing transport coefficients are required to quantitatively predict the phase-ordering dynamics of any given system, a great deal can be gleaned just from the shape of the free-energy landscape. We demonstrate how to extract the most information concerning phase-ordering phenomenology from a knowledge of a system's free-energy function, or phase diagram. Many putative pathways to equilibrium can be ruled out on the grounds of the second law of thermodynamics. In some parts of the phase diagram, these considerations are sufficient to completely determine the phase-ordering process without ever having to calculate a transport coefficient, even when three phases are present. The results include a large number of regions of the phase diagram with distinct phase-ordering kinetics, and some surprisingly elaborate routes to the equilibrium state. A process is found whereby a crystalline condensation nucleus becomes coated with a shell of gas, buffering it from a majority metastable liquid phase. Our results, based on thermodynamic arguments, are supported by numerical solution of model *B*, which describes diffusive phase-ordering kinetics. Some of our predictions are tested against experimental observations of colloid-polymer mixtures, described in more detail in the preceding paper [F. Renth, W. C. K. Poon, and R. M. L. Evans, *Phys. Rev. E* **64**, 031402 (2001)]. A compact notation is developed to represent intricate phase-ordering pathways.

DOI: 10.1103/PhysRevE.64.031403

PACS number(s): 64.75.+g, 64.60.My, 82.70.Dd

I. INTRODUCTION

Considering that the existence of phase transitions was explained in the nineteenth century, it is perhaps surprising that their kinetics are not yet fully understood. There is no shortage of academic interest in the subject [1–10], nor of applications. In metallurgy and materials science, determining the dynamics of phase separation after a quench is of considerable technological importance for controlling mesoscopic texture [11]. Also, the rate at which metastable states evolve towards equilibrium determines the longevity (or “shelf life”) of many industrial products.

The prediction of phase-ordering kinetics presents a considerable challenge to condensed matter physics. To be sure, many phenomenological models exist. However, determining which is most appropriate to a given system is something of an art since, unlike equilibrium thermodynamics, no general formalism is known for deriving macroscopic behavior from microscopic properties. The experimental characterization of phase-ordering processes is also problematic. Unlike bulk thermodynamic properties, which are easily measured, the processes of phase ordering, particularly in the early stages, take place on microscopic length and time scales that are not readily accessible. Additionally, to prepare a well-characterized initial state, the system must be quenched within this microscopic time scale. As a result of these theoretical and experimental difficulties, the study of phase-ordering kinetics is still in its early stages. Of all phase-ordering phenomena, only a relatively small proportion have been thoroughly investigated. For example, systems with phase diagrams exhibiting a triple- or higher-phase coexistence are ubiquitous. Yet the overwhelming majority of existing studies of kinetics are concerned with two-phase regions.

In the preceding paper [16] many of the experimental difficulties were overcome in collecting comprehensive data on the kinetics of ordering in a system approaching three-phase equilibrium. The strategy was to study a complex fluid with

a phase diagram that mimics that of a simple atomic substance such as argon, but the kinetics of which are much easier to observe. The experimental system chosen was a colloid-polymer mixture. The equilibrium phase behavior of these mixtures is well established [12–14]. Less is known about the detailed kinetics of their phase ordering in a two-phase region [15] and, until the recent observations [16], next to nothing was known of the approach to three-phase equilibrium. The recent observations [16] allow us to probe the phenomenology of phase ordering in some detail. They reveal a surprising amount of diversity in the chronological order of events during the approach to three-phase equilibrium in samples with very similar overall composition.

Our aim, then, is to understand the kinetics of colloid-polymer mixtures in and around the three-phase region. The underlying physics has important generic implications. This is because the relevant features of the free energy and phase diagram of colloid-polymer mixtures, which we shall discuss, are shared by many (even most) other complex fluids. In addition, an exact mapping can be constructed from the properties of a colloid-polymer mixture to those of a standard pedagogical system in a heat bath. In particular, the polymeric activity is exactly analogous to the reciprocal of temperature in an atomic system, and polymeric concentration is therefore related to latent heat, while colloidal concentration maps onto atomic density.

We investigate the thermodynamics of processes which lead from an initial homogeneous nonequilibrium state towards a final three-phase equilibrium. The study will give rise to a scheme which, as well as classifying various kinetic regimes, turns out to have considerable predictive power. The framework relies on no phenomenological assumptions. Instead we follow the approach that Cahn applied to simpler systems [17], to determine the sign of the entropy change associated with different processes, thus ascertaining which kinetic pathways are forbidden.

The rest of the paper is organized as follows: We briefly

review the equilibrium phase behavior of colloid-polymer mixtures in Sec. II. In Sec. III we study the thermodynamics of phase transition kinetics in colloid-polymer mixtures. The results of that discussion are used in Sec. IV to classify and catalog the regimes of kinetic behavior in the colloid-polymer phase diagram. Implications for phase transitions in other substances are discussed in Secs. V and VI. Some of the predictions of Sec. IV are tested against a simple numerical model in Sec. VII, and in Sec. VIII we summarize and conclude.

II. COLLOID-POLYMER MIXTURES

The addition of a nonadsorbing random-coil polymer to a sterically stabilized suspension of quasi-hard-sphere colloidal lattices induces an effective pair potential between the particles, known as the depletion interaction [18]. Where two of the spherical colloid particles are so close together that the smaller polymer molecules cannot fit between them, the polymeric concentration (and therefore the osmotic pressure) between the spheres is reduced. The range and depth of this effective attraction can be tuned by choosing the size and concentration of the polymer coils [19,12]. In this way, the topology of the phase diagram can be made to mimic that of simple atomic/molecular substances, with gas, liquid, and crystal regions, as well as a point of triple coexistence [13].

Thus, the polymeric chemical potential μ_p can be considered to parametrize the effective strength of particle-particle attractions in the colloidal suspension, in the same way that the temperature parameter $\beta \equiv 1/k_B T$ does for systems of particles with a real energetic interaction potential. While μ_p^{-1} plays the role of temperature in the colloid-polymer mixtures, temperature itself is of only minor importance, since all interactions in the system are repulsive and, in principle, hard. In practice, some details of the polymer-solvent interactions are not purely steric, so that some temperature dependence is evident. However, energetics are irrelevant in the sense that the phase transition dynamics in this system is not limited by diffusion of latent heat, since entropy is dominated by the solvent bath, which induces Brownian dynamics in the suspended particles.

By choosing the numbers of colloidal particles, polymer molecules, and solvent molecules in a sample, a state of three-phase coexistence can be orchestrated. Once such a sample has been prepared; it can be homogenized into a uniform, nonequilibrium, amorphous state. The subsequent kinetics, as it returns to coexistence, were measured in the preceding paper [16] and are analyzed theoretically in the rest of this paper.

III. THERMODYNAMICS OF PHASE ORDERING

A. Background

A homogeneous system out of equilibrium, which is initially in a forbidden (multiphase) region of the phase diagram, must eventually attain thermodynamic equilibrium by arriving on the phase boundaries. Out of the many available paths through phase space, it is not generally obvious which one it will take on its approach to the equilibrium state. Cahn [17] showed how the shape of a mean-field free-energy curve

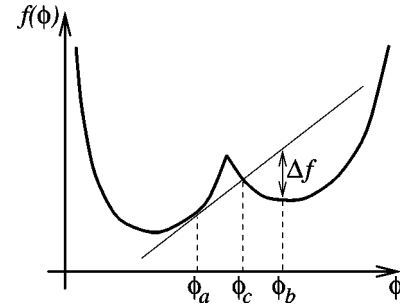


FIG. 1. Example of the construction on a (mean-field) free-energy curve, with concave parts, giving the free energy available to create an infinitesimal amount of composition ϕ_b in a metastable phase at composition ϕ_a .

(that is, the free energy of a uniform phase with no significant heterogeneities) alone can be used to narrow the possibilities, ruling out some pathways. Of course, to ascertain the exact course that the system will follow, one must calculate *both* the rates of nucleation *and* the subsequent growth rates (either of which may exhibit highly nontrivial behavior [7–10,20]) for various processes. That would require a detailed knowledge of the mobilities and gradient energies for various order parameter fields, as well as an ansatz for the phenomenological equations of motion. However, without a knowledge of any such kinetic parameters, Cahn [17] showed how to limit the possibilities, simply by determining which condensation nuclei carry an entropic cost, and must therefore dissolve in the metastable majority phase.

The principle, which was used [17] to investigate nucleation in substances with a free energy that is a function of a single composition variable, is as follows. Consider a system with free-energy density $f(\phi)$ as a function of the uniform composition ϕ , given in Fig. 1. If the composition is initially uniform at $\phi = \phi_a$, it can be shown (simply by conservation of material) that the free energy available to create an infinitesimal amount of a second phase at concentration ϕ_b is given by the distance Δf from the tangent. Thus, nucleation of a phase with composition $\phi < \phi_c$ cannot take place, as it would raise the system's free energy, and must therefore dissolve in the majority phase. Despite the simplicity of this principle, it can be applied to obtain generic and sometimes counterintuitive results. For example, for certain free-energy curves, the nucleation of the final, stable states is forbidden until after the formation of metastable precursors [17].

B. Free-energy landscapes

The whole basis of this formalism relies on the existence of free-energy curves which are not globally convex. Such curves (whose shapes give rise to the expression “free-energy landscape”), if misinterpreted, might be dismissed as unphysical, as we now discuss. After sufficient time, the system will attain thermodynamic equilibrium by partitioning into coexisting regions of differing compositions. The free energy of this equilibrated system is required to be a convex function of its mean composition, by virtue of the positivity of susceptibilities [21]. Indeed, the construction in Fig. 1 demonstrates that the global free energy is not minimized unless all tangents lie below the curve. Nevertheless, at early

times, a finite system (or a finite part of an infinite system), quenched to $\phi = \phi_a$, will explore only a subset of its configurations—those attributable to the metastable initial phase [22]. During this time, any order parameters that distinguish the two phases may be regarded as quenched (as opposed to annealed) variables.¹ Thus, before the second phase nucleates, the left-hand well in Fig. 1 is the correct form of the free energy. For instance, the second derivative of this curve gives the experimentally measurable susceptibility in the metastable state. In order for this description to apply, where fluctuations within one well of the free energy are distinguished from fluctuations that form condensation nuclei, the equilibration time (the time to establish a Boltzmann distribution) in the metastable state must be much less than the nucleation time (after which a significant fraction of the system feels the presence of nuclei). Given that this criterion is satisfied, the function in Fig. 1 is well defined.²

C. Treatment of two components

For systems with several density variables, the tangent construction depicted in Fig. 1 has a straightforward extension. The free energy becomes a (hyper-)surface spanned by the composition variables, and entropically favored condensation nuclei must lie below its tangent (hyper-)plane. However, as this becomes difficult to visualize, we shall demonstrate for colloid-polymer mixtures how the simple, one-component method may be rigorously applied to more complex systems. By the Gibbs phase rule, with two independent concentration variables, a region of triple coexistence is possible. Hence the principles described above, originally applied to a pure system [17], may be expected to classify a richer diversity of behaviors.

To classify the possible kinetics of colloid-polymer mixtures, we reason as follows. The free-energy surface $f(\phi, n_p)$, which is a function of both colloidal and polymeric concentrations,³ can be mapped by a Legendre transform onto a semigrand potential density $\Omega(\phi; \mu_p)$. At equilibrium, this function is minimized (subject to conservation) with respect to colloidal concentration ϕ alone. In that sense it is a function of one variable, while $1/\mu_p$ acts as a temperaturelike parameter controlling the shape of that curve. The semigrand potential is a standard tool of equilibrium thermodynamics. During phase ordering, however, it is not obvious that the polymeric chemical potential can be treated as an external parameter, since it is generally nonuniform. An exception is in the initial state which is homogeneous, so μ_p takes a single value. Thus the semigrand potential is a well-

defined curve at both the beginning and end of phase ordering.

The method for establishing the legality of a nucleation event, outlined above and depicted in Fig. 1, applies to a free-energy curve (under given imposed conditions such as temperature) which is a function of a single composition variable. It would be convenient to apply it to the one-dimensional semigrand potential, in which the control parameter is actually the chemical potential of another conserved species. Happily, the method still holds in this case, as we now show. Let $F_{\text{init}} = Vf(\phi_a, n_a)$ be the total canonical free energy of the system of volume V , initially at a homogeneous colloidal concentration ϕ_a and polymeric number density n_a . If a small volume V_b of the system acquires the composition (ϕ_b, n_b) , the remainder must change in composition $(\phi_a, n_a) \rightarrow (\phi_a + \Delta\phi_a, n_a + \Delta n_a)$ so as to respect conservation of material, as expressed by

$$\phi_a V = (\phi_a + \Delta\phi_a)(V - V_b) + \phi_b V_b,$$

$$n_a V = (n_a + \Delta n_a)(V - V_b) + n_b V_b.$$

Hence the canonical free energy of the compound system becomes

$$F_{\text{comp}} = (V - V_b)f(\phi_a + \Delta\phi_a, n_a + \Delta n_a) + V_b f(\phi_b, n_b).$$

So the change $\Delta F = F_{\text{comp}} - F_{\text{init}}$ in the limit $V_b/V \rightarrow 0$ is given by

$$\Delta f \equiv \frac{\Delta F}{V_b} = f_b - f_a - (\phi_b - \phi_a)\mu_c - (n_b - n_a)\mu_p, \quad (1)$$

where $f_{a,b} \equiv f(\phi_{a,b}, n_{a,b})$, and μ_c and μ_p are the colloid and polymer chemical potentials, respectively, $\mu_c = (\partial f / \partial \phi)_n$ and $\mu_p = (\partial f / \partial n)_\phi$. Equation (1) has the form $\Delta f = f_b - \pi(\phi_b, n_b)$, where $\pi(\phi, n)$ is the equation of the plane tangent to $f(\phi, n)$ at (ϕ_a, n_a) . If Δf is negative, the nucleation process is favorable, whereas the nucleus must redissolve if $\Delta f > 0$. The marginal case, when no canonical free energy is available for driving nucleation (but neither is there a cost to it) of a phase with composition (ϕ_b, n_b) , is given by $\Delta f = 0$ in Eq. (1). Thus the boundary to the region of phases that may nucleate is given by

$$f_b = f_a + (\phi_b - \phi_a)\mu_c + (n_b - n_a)\mu_p.$$

That is, where the free-energy surface is intersected by its tangent at the initial state. In terms of the semigrand potential density $\Omega \equiv f - \mu_p n$, this criterion reads

$$\Omega_b = \Omega_a + (\phi_b - \phi_a)\mu_c, \quad (2)$$

which is the point of intersection with the tangent line [since $\mu_c = (\partial \Omega / \partial \phi)_{\mu_p}$] on the curve $\Omega(\phi)$, equivalent to ϕ_c in Fig. 1.

Thus Cahn's recipe applies, unmodified, to the semigrand potential curve, with μ_p a control parameter whose initial value, though uniform, differs from its value at equilibrium. In fact μ_p is initially greater than its equilibrium value, since the phase-ordering process is (partly) driven by expansion of

¹In practice, all quenched variables (those which define a constraint on a system) are time-scale dependent since, on cosmological time scales, all constraints will yield to the increase of entropy.

²The criterion can be violated if $f(\phi)$ has negative curvature, giving rise to local instability. We note, however, that the phenomenological description of spinodal decomposition [23], which relies on such functional forms, is not without content. For an unambiguous definition of such functions, see [24].

³ ϕ is the dimensionless colloid volume fraction and n_p is the number density of polymer coils.

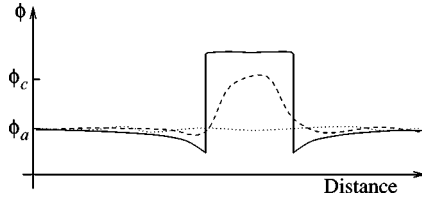


FIG. 2. Schematic illustration of nucleation.

the free volume of the polymer gas by overlap of depletion zones around colloids [18,19].

D. Description of phase ordering

Consider then the progress of phase ordering in a system whose semigrand potential is initially represented by the curve in Fig. 1. (Read Ω for f in the figure.) The initial colloidal concentration is uniform at $\phi = \phi_a$, as shown by the dotted line in Fig. 2, which depicts a one-dimensional slice through the system. Though fluctuations around the mean value ϕ_a will occur in the system, they must all decay, until a (sufficiently large [25]) region spontaneously exceeds the concentration ϕ_c , as shown by the dashed line in the figure. Growth of that region is entropically favorable, so material will flow into it, increasing its concentration and size, while depleting the local surroundings. As the environment is reduced in concentration, below ϕ_a in Fig. 1, the tangent rotates clockwise, reducing the driving force for further growth of the nucleus. A sharp interface will quickly form between the two concentrations that share a common tangent, and are therefore locally in equilibrium, as shown by the solid line in Fig. 2. The distant bulk of the majority phase remains at its initial concentration, and so a gentle concentration gradient exists, driving diffusion of material onto the surface of the growing condensation nucleus.

Though a continuous range of concentrations exists in the nonequilibrium system (solid line, Fig. 2), it is clear that two phases may be unambiguously identified, as they are separated by a sharp interface. Such an interface can exist if the free-energy curve has a corresponding pair of cotangential concentrations, whether or not they transpire to be the values of absolute stability. In fact, since the two phases are separated by a (unstable) point of concavity on the free-energy curve, a continuous gentle concentration gradient between them cannot be sustained. This provides an unambiguous definition of a phase in our nonequilibrium systems, which we shall henceforth adopt. Two phases are distinct if and only if a continuous diffusion gradient could not (with appropriate fluxes at the boundaries) be maintained between them (or, equivalently, if they are separated by a point⁴/interval of concavity on the free-energy curve).

IV. THE REGIMES OF BEHAVIOR

Consider again the initially homogeneous system represented by the dotted line in Fig. 2. If its concentration had been slightly below ϕ_a , a growing nucleus of the second

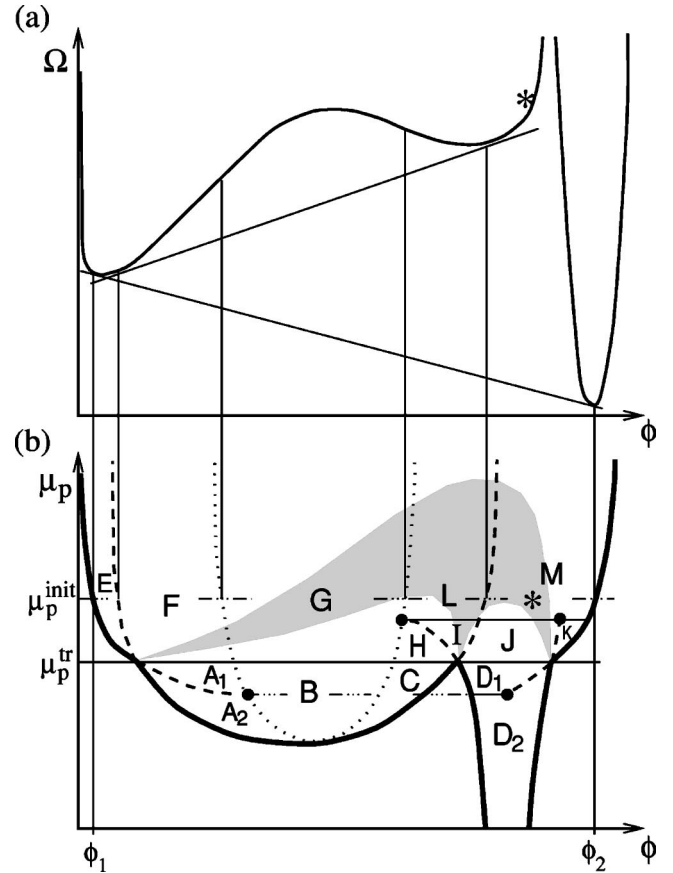


FIG. 3. (a) Semigrand and potential density as a function of colloidal concentration for a polymeric chemical potential μ_p^{int} . All pairs of cotangential points are shown. They correspond to the coexisting stable (heavy lines) and metastable (dashed lines) phases which, with the spinodal (dotted), divide the phase diagram (b) into different kinetic regions (A to M), shown in the (ϕ, μ_p) plane. The locus of metastable liquids whose equilibrium is three-phase is shaded gray.

phase could still have formed, since the tangent in Fig. 1 would still lie above part of the free-energy curve. Only if the initial concentration were below the point of cotangency would a nucleation of the second phase be forbidden (entropically unfavorable). Thus, cotangential concentrations on the free-energy curve delimit the regimes of allowable nucleation events. Some of these cotangencies also define the binodals [phase boundaries, heavy lines in Fig. 3(b)] on the equilibrium phase diagram, but others are extensions of the binodals into the coexistence regions [dashed lines in Fig. 3(b)]. An example semigrand potential curve at the initial polymeric chemical potential μ_p^{int} in Fig. 3(a) shows the cotangencies corresponding to the nucleation boundaries in the schematic phase diagram, Fig. 3(b).

The boundaries, thus derived from cotangencies on the semigrand potential curve, divide Fig. 3(b) into many regions, each with different possibilities for its initial phase-ordering kinetics. Note that the mean-field gas-liquid spinodal is also marked. Within the spinodal region, the initial system is locally unstable, so its kinetics are characteristic of a distinct regime. The regions of potentially distinct initial

⁴Such as the cusp in Fig. 1.

kinetics are labeled A to M in the diagram. As an example, consider a system which is initially homogeneous at the composition marked (*) in Fig. 3, which is in region M . The three wells in the semigrand potential curve of Fig. 3(a) correspond to colloidal gas, liquid, and crystal phases, in increasing order of concentration ϕ . The initial state (*) corresponds to a liquid phase, and is to the right of the liquid-gas common tangent. Therefore a tangent to the point (*) lies below the gas well, so the formation of gas bubbles is disallowed. However, free energy is available for the formation of crystallites, so that must be the first process to happen. Observe, though, that no double tangent can be drawn between the liquid and crystal wells. Hence a crystallite, once formed, cannot attain local equilibrium with the surrounding liquid phase, but must continue to deplete its concentration until the crystallite is surrounded by colloidal gas. A second interface must form between that gas and the surrounding liquid, since they are distinct phases, as defined above. Thus, although nucleation of gas alone is initially disallowed, the crystallites that nucleate must be surrounded by a shell of gas phase. Only after the majority liquid phase has been sufficiently depleted by this process (so that its tangent rotates to cross the gas well) can further gas nuclei form, independently of crystallites.

With a knowledge of the features of the free-energy landscape alone, not only can such interesting scenarios be predicted for the initial stages, but also the final state is predetermined. The compositions and volumes of the final coexisting phases are simply found by applying the lever rule to the equilibrium phase diagram (in terms of conserved polymeric concentration n_p), and hence the final value of the polymeric chemical potential is determined. This may be above, below, or equal to the triple value μ_p^{tr} , depending on the initial composition and on the polymer-colloid size ratio (which parametrizes the effective colloid-colloid interaction). So, for states initially above the triple line, $\mu_p^{\text{init}} > \mu_p^{\text{tr}}$, the regimes denoted E to M , which are distinguished by their initial behaviors, are further subdivided threefold, depending on whether their final state lies above, below, or on the triple line. To illustrate this subdivision, the locus of initial states, whose equilibration will take them onto the triple line, is shown schematically in Fig. 3(b), shaded gray. For different polymer-colloid size ratios, the boundaries of this locus can intersect different regions, though always above the triple line.

A. Validity

Note that the thermodynamic procedure described in Sec. III C assumes uniform concentrations within each spatial region (the infinitesimal condensation nucleus and the surrounding medium), and takes no account of surface energies. In fact, these assumptions are not at all restrictive, since heterogeneities (which arise due to localized depletion around each nucleus) and surface energies can only increase the free energy of the compound system (the system containing a condensation nucleus). These effects therefore tend to suppress a nucleation event, but do not move the boundaries of its allowed region. These boundaries delineate the limits of allowed formation of the *most favorable* nucleus—one which

pays no free-energy cost for heterogeneities, and is sufficiently large for the free energy of its bulk to outweigh that of its surface [25].

The only approximate features of our analysis (other than the *precise* locations of the boundaries in Fig. 3) are the following assumptions: (i) That all possible states lie on a relatively simple free-energy landscape (for a uniform phase). We have therefore neglected the highly nonergodic glass [26,6,27–29] and gel [30] states. (ii) That the topology of the semigrand potential curve is known. This is rigorous until the first nucleation event. However, for the *two-stage* process described above, where a “shell” of gas forms *subsequent* to crystallization in region M , an approximation is invoked. In that case, the polymer is required to be sufficiently fast to maintain its equilibrium with the bulk, thus ensuring that the advancing crystal interface remains in region M where it cannot coexist with liquid.

B. Compact notation

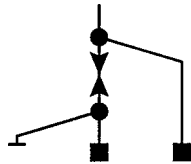
Though some details of the phase-ordering kinetics of colloid-polymer mixtures cannot be determined without a phenomenological model, we have identified a large number of regions in the phase diagram, with distinct regimes of behavior in the initial and final stages. With such a large number of possible scenarios to catalog, it is advisable to devise a compact notation by which to represent the order of events.

Four generic processes or events are of interest, which we shall represent by the following symbols: formation of a new phase (●), spinodal decomposition into a pair of new phases (s), the complete disappearance of a phase (when neighboring regions encroach upon it by interfacial motion, i.e., evaporation, condensation, etc.) (-), the survival of a phase in the final equilibrium state (■). Each of these processes may occur within a region of colloidal gas (g), liquid (l), or crystal⁵ (χ) (identified unambiguously by the definition above), and this will be indicated by the lateral position of the symbol (g, l, χ from left to right). Any two such processes (α and β , say) may be causally related in one of the following ways: (1) Either may occur, independently of the other. (2) β cannot occur until after α . (3) Given α , β must follow. In the latter two relationships, α precedes β , but the dependence of one on the other is opposite in (2) and (3). Hence, with time represented vertically (increasing down the page) relationships (2) and (3) can be represented as oppositely directed line segments, while relationship (1), which has no causal dependence, is shown as an undirected line segment, thus

- 
May happen in either order.
- 
 β cannot occur until after α .
- 
Given α , β must follow.

⁵Additionally, spinodal decomposition takes place in the unstable region *between* g and l .

The arrow may be thought of as a mathematical “implies” sign. An upward arrow would tend to represent a slow succession of events, since the second nucleation process cannot take place until conditions in the majority phase have changed sufficiently, under the influence of the preceding process.⁶ A downward arrow would tend to represent a very rapid succession of events, such as the immediate formation of gas, necessitated by the nucleation of crystals, as in region M described above. In that particular example, arrows would point in *both* directions, since gas *cannot* form until crystals nucleate, but is then *compelled* to form. Thus, the dynamics in the part of region M below the gray locus in Fig. 3 (which will end in crystal-liquid coexistence) is represented by the following pathway diagram:



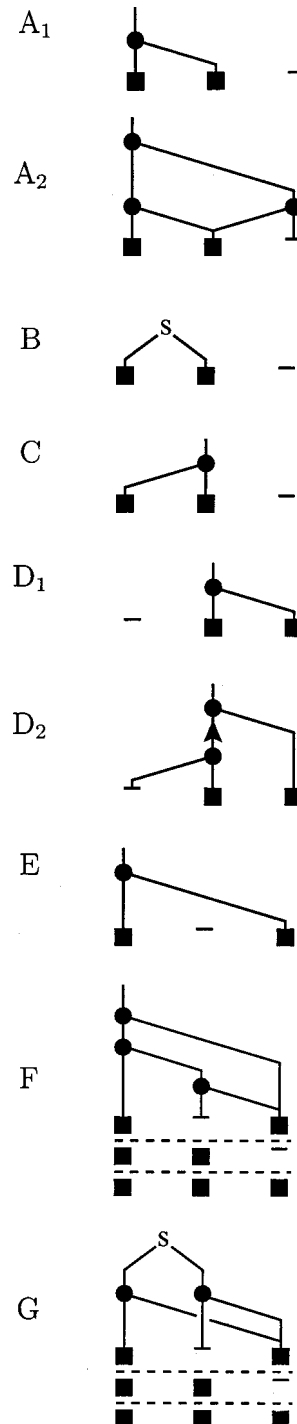
This diagram indicates a strange scenario. The mixture begins as a homogeneous liquid, and ends in crystal-liquid coexistence. However, on the way, gas phase *must* appear (an arrow in the diagram points to its formation) and then disappear.

Since we have only determined which pathways are thermodynamically forbidden, or else *possible*, as opposed to which scenario will *actually* result from a particular equation of motion, a pathway diagram contains all possible scenarios. Hence any subdiagram, obtained by removing and/or rearranging parts of a pathway diagram, is thermodynamically allowed, so long as it contains all final states (■), includes any process pointed to from another process in the subdiagram, and does not swap processes on a directed segment. In some cases, including the example above, the diagram cannot be reduced, so the problem of determining the order of events during phase separation is solved outright. The complete set of pathway diagrams, cataloging the expected kinetics of colloid-polymer mixtures in all regions of the phase diagram, is given in Sec. IV C. In some cases (cited in Sec. IV C), the putative behavior is already recorded in the literature. Note that the derivation of these diagrams does not require precision in the mean-field semigrand potential used, but relies only on its topological features, which can mostly be inferred from the phase diagram.

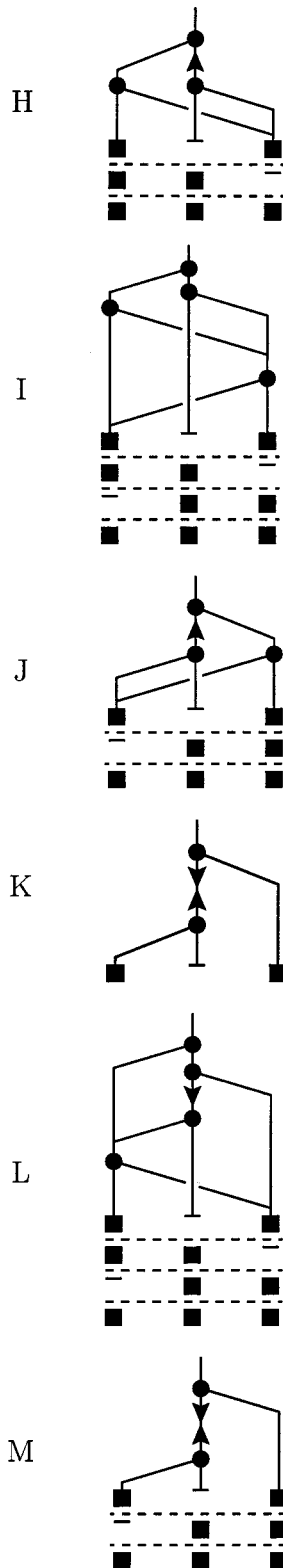
C. Catalog of kinetic regimes in the colloid-polymer phase diagram

Using the rules set out above, the order of thermodynamically allowed events during phase ordering is determined for each region of the colloid-polymer phase diagram [Fig.

3(b)]. The initial and final states, and allowable intermediate paths, are summarized in the following pathway diagrams. Gas, liquid, and crystalline phases appear from left to right, respectively, and chronological order advances from top to bottom within each diagram. We recall that nonergodic (i.e., gel and glass) phases are neglected by the theory. For regions which are *intersected* by the locus of quenches that equilibrate to three-phase final states [shaded gray in Fig. 3(b)], the various alternative final states are shown in the corresponding pathway diagram, separated by dashed lines.



⁶However, some rapid *heterogeneous* secondary nucleation may take place, close to the initially formed nuclei, before conditions in the bulk have changed to favor the secondary process.



Let us briefly consider some of these pathway diagrams. The diagram for region *B* corresponds to classical spinodal decomposition [23]. That theory, in common with the present analysis, assumes local quasiequilibrium, allowing information to be derived from a free-energy function. It therefore also neglects nonergodic (glassy) phases, which can in practice modify the process [5,6].

The pathway diagram for region *E* represents straightforward nucleation of a crystal phase from the majority super-saturated gas. The diagram for the part of region *F* above the three-phase locus (i.e., with the first alternative ending: gas-crystal equilibrium) contains the simple region *E* pathway as a subdiagram. However, it also contains the possibility of crystal formation proceeding via an intermediate metastable liquid phase. Such a process has been studied in terms of its influence on both nucleation [7] and subsequent growth [31,20] mechanisms. A further subdivision of this part of region *F* was predicted [20], with two regimes corresponding to the two subdiagrams.

The process represented by the pathway diagram for the part of region *G* above the three-phase locus (with the first alternative ending of the diagram) has been evidenced in recent Brownian dynamics simulations of colloid-polymer mixtures [32]. Although the final equilibrium state is gas-crystal coexistence, a spinodal-like instability led to the appearance of a texture of high and low density amorphous regions during the early stages of these simulations. Crystals subsequently formed in one of these regions (the higher density region in this case).

The diagram for region *I*, because it is the largest diagram, contains the least information. It only shows that all things are possible in this region, since no order of events is thermodynamically forbidden. The actual kinetically determined pathway remains a mystery. To predict the behavior in this region requires the calculation of nucleation rates (many of which have been estimated for this and other regions of the phase diagram [10]) and growth rates.

The pathway diagram for the part of region *M* below the three-phase locus is discussed in Secs. IV and IV B, and modeled in Sec. VII.

It is well known [13,19] that the phase diagram for colloid-polymer mixtures changes in topology if the polymer-colloid size ratio is below about 0.25. In that case, the equilibrium gas-liquid binodal disappears entirely within the gas-crystal coexistence region, so that gas-liquid coexistence is only a metastable phenomenon and no triple point exists. Nevertheless, the common tangent can be constructed between the gas and liquid minima of the free energy, so that this metastable binodal could be mapped out on the phase diagram, as, one imagines, could the metastable liquid-crystal coexistence boundaries.⁷ So all the metastable coexistence boundaries that appear above the triple line in Fig. 3(b) should remain in the small-polymer case, delineating the same regimes of behavior (*E* to *M*). Regions *A* to *D*, on the other hand, should no longer appear.

V. APPLICATION TO OTHER “LIATROPIC” SYSTEMS

Our analysis of the phase-ordering pathways accessible to a system with three free-energy minima is not restricted to colloid-polymer mixtures. There are many liotropic systems comprising two components in an incompressible solvent.

⁷The liquid side of such a liquid-crystal metastable binodal would have to begin and end on the gas-liquid spinodal.

Given that the phase diagram has the topology of Fig. 3(b) in terms of the concentration ϕ of the slower component, and that the dynamics is Brownian so that ordering is not limited by heat transport, then the above pathway diagrams embody the admissible behaviors. For example, the phase diagram of mixtures of colloidal boehmite rods and flexible polymers [33] has the same topology as that of our colloid-polymer mixtures. We therefore expect phase ordering to follow the above pathway diagrams, taken to represent (from left to right) the dilute isotropic, concentrated isotropic, and nematic phases.

Note that each pathway diagram shown initiates in one of the amorphous phases (gas, liquid, or unstable). For practical reasons, phase ordering of colloid-polymer mixtures is never initiated in a uniform nonequilibrium crystalline state. We have therefore not presented diagrams initiated by a line in the rightmost column. However, for other isotropic systems, sharing the phase-diagram topology of Fig. 3(b), additional such pathway diagrams may be relevant, representing a quench into the high-concentration, ordered phase.

For systems with more elaborate phase diagrams, our methodology can again be used, extending phase boundaries into multiphase regions to delineate kinetic regimes. The elements of the pathway diagrams defined above (with more columns if more than three phases are to be represented) should suffice to summarize the results in a set of new diagrams appropriate to the given system.

VI. CORRESPONDENCE TO ATOMIC AND SIMPLE MOLECULAR SUBSTANCES

We noted, in Secs. I and II, the similarity between the equilibrium phase diagram of a colloid-polymer mixture and that of an atomic or simple molecular substance, if reciprocal temperature is substituted for polymeric activity. It is interesting now to investigate the exactness of that correspondence in terms of kinetics.

All interactions in the colloid-polymer mixture (CPM) are approximately hard and repulsive. Thus, the system has no characteristic energy scale, so temperature is an irrelevant field. The two conserved fields, colloidal and polymeric concentration, can be mapped onto a purely colloidal system with effective interactions parametrized by polymeric activity. Similarly a simple molecular substance (SMS) is governed by two conserved fields: material density and energy density; the latter can be described in terms of a temperature which parameterizes the interactions of the former.

For an ideal polymer (as approximated at the polymeric θ point), the depth of the effective colloid-colloid interaction potential is proportional to the concentration (number density) of polymer n^{free} in the free volume allowed to it by the colloid. This is equal to the ideal polymeric activity a_p , and related to the actual polymeric concentration n by $n = \alpha(\phi)n^{\text{free}}$, where $\alpha(\phi)$ is the fraction of the total volume available to the polymer. The behavior of a SMS depends on the interaction potential, measured in units of $k_B T$. Thus, in physically relevant units, the depth of the potential is proportional to $1/T$. So it seems reasonable to make the correspon-

dence $T \leftrightarrow a_p^{-1}$. Both quantities are nonconserved, and take values in the range $[0, \infty]$.

Nucleation of a denser phase tends to be exothermic in a SMS, and therefore locally increases the temperature. Correspondingly in a CPM, such an event locally increases the free volume fraction α and therefore lowers the activity a_p .

Subsequent to this, in a SMS, the temperature field equilibrates diffusively, whilst respecting conservation of energy. For differences ΔT from the ambient temperature, that conservation is expressed (in the absence of further phase changes) by

$$\int d^3r C \Delta T = \text{const},$$

where the integral is over the whole system, and C is the heat capacity (at constant pressure) per unit volume, which appears inside the integral since it is a property of the different phases present. In a CPM, the polymer concentration, and hence also its reciprocal activity, equilibrates diffusively, whilst respecting conservation of the number of polymer molecules. In terms of small changes $\Delta(a_p^{-1})$ in the reciprocal polymeric activity, that conservation can be written

$$\int d^3r a_p^2 \alpha(\phi) \Delta(a_p^{-1}) = \text{const}.$$

This and the accompanying diffusion equation for $\Delta(a_p^{-1})$ hold only for small changes from the ambient activity, but that is also the case for the SMS temperature field, since C is T dependent.

Finally, consider the latent heat of a phase change in a SMS. Since heat corresponds to polymer number in a CPM, we see that the latent heat per unit volume, measured at constant temperature, corresponds to $a_p \Delta \alpha$, where $\Delta \alpha$ is the change in free volume fraction, brought about by the rearrangement of the colloidal lattices.

In summary, the thermodynamics of phase ordering of colloid-polymer mixtures, investigated in this paper, applies also to simple molecular substances, with the following exact correspondences:

simple molecular substance \leftrightarrow colloid-polymer mixture,

heat \leftrightarrow polymer number,

temperature $\leftrightarrow a_p^{-1}$,

heat capacity/unit volume $\leftrightarrow a_p^2 \alpha$,

latent heat/unit volume $\leftrightarrow a_p \Delta \alpha$.

Thus a consideration of kinetic regimes in the ϕ - n plane for a colloid-polymer mixture translates into the density-energy plane for a molecular liquid undergoing adiabatic change at constant volume. The approach to equilibrium of such a system—subtriple liquid benzene in an insulating container at fixed volume—is discussed in Ref. [25], where

experimental data are reviewed, and entropy changes are considered for processes equivalent to parts of diagrams *I*, *J*, and *K*.

VII. NUMERIC MODELING

A. A toy model

We have predicted various kinetic regimes from the qualitative features of a system's free energy, irrespective of its dynamic phenomenology. Since any model of phase-ordering dynamics should display the predicted behavior, we test the theory using the simplest: model *B* [34], or the Cahn-Hilliard equation [35]. Using numeric quadrature, we observe the model's behavior in one of the more exotic putative kinetic regimes.

In this purely diffusive model, the single order parameter $\phi(\mathbf{r})$ (here representing colloidal concentration) is conserved. It therefore respects a continuity equation

$$\dot{\phi} = -\text{div } \mathbf{j}$$

with the flux \mathbf{j} responding to the gradient in the chemical potential μ , in proportion to a mobility Γ

$$\mathbf{j} = -\Gamma \text{grad } \mu.$$

As the system is inhomogeneous, its free energy F is a *functional* of the field $\phi(\mathbf{r})$, so the chemical potential (derivative of free energy with respect to concentration) is a functional derivative

$$\mu = \frac{\delta F[\phi(\mathbf{r})]}{\delta \phi(\mathbf{r})}.$$

At a given point in space, the free-energy density (in this case, a semigrand potential) is some thermodynamic function $\Omega(\phi)$ of the local concentration, such as that shown in Fig. 1. Additionally, there is a penalty (always positive) to spatial variations of ϕ , which must be included, as it is the source of surface tension between phases, though it does not modify the thermodynamic phase diagram. So F has the form

$$F[\phi(\mathbf{r})] = \int d^3r \left\{ \Omega(\phi) + \frac{1}{2} \kappa |\nabla \phi|^2 \right\}.$$

With a suitable choice (discussed below) of the curve $\Omega(\phi)$ and the parameters Γ and κ , these equations were quantized in space and time. The time step and grid parameter were each reduced until they had no effect on the results. A deterministic algorithm was used which rigorously conserved material both in the bulk and at the boundary. Spherical symmetry was imposed on the system, so that three spatial dimensions were modeled by a linear set of data points (each datum representing the amount of material within a spherical shell).

It is known that, at low concentrations, $\Gamma \propto \phi$ (this is required to make the diffusivity of an ideal gas independent of its concentration). However, since we are concerned less with the ideal-gas limit than with numerical efficiency, we choose a constant mobility, recalling that the results should

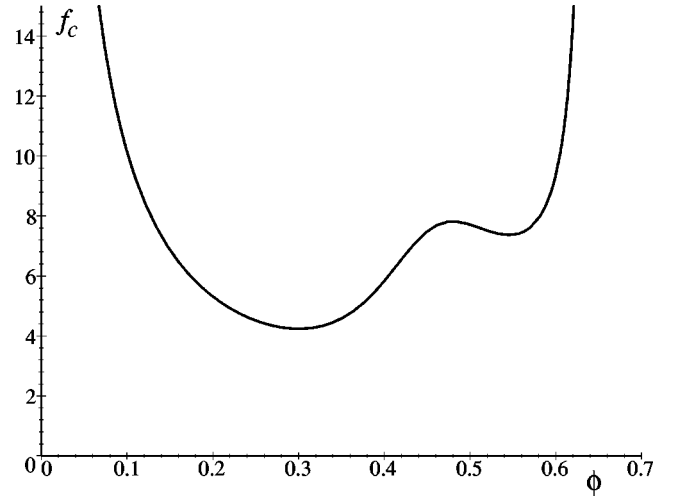


FIG. 4. The “colloidlike” free-energy density $f_c(\phi)$ is a simple algebraic function, $\phi^{-1} + (0.64 - \phi)^{-1} [1 + b^2(\phi - c)^2]^{-1}$ with two wells. The barrier separating the wells has a sharpness set by $b = 10$ and a position $c = 0.45$.

be qualitatively independent of the precise phenomenology. As this constant serves only to scale time, it is set to unity without further loss of generality.

For a given $\Omega(\phi)$, the constant κ determines the thickness of an interface (the length scale of its structure, above which it appears sharp), which is also the length scale of a critical nucleus. As this is the only length scale other than system size, it can be fixed at will without loss of generality. In our case $\kappa = 200$ was chosen, to give interfacial widths of order unity.

The $\Omega(\phi)$ curve employed has the *qualitative* features of a colloid-polymer mixture's semigrand potential, while being both differentiable and algebraically simple for numerical efficiency. Following Ref. [19], we write the bulk *canonical* free-energy density $f(\phi, n_p)$ in two parts: that of a pure colloid in the absence of polymer $f_c(\phi)$, and that of an ideal gas of polymer $f_p(n_p, \phi)$ of number density n_p , confined to a fraction $\alpha(\phi)$ of the volume, thus

$$f = f_c(\phi) + f_p(n_p, \phi).$$

Since pure colloid can exist in two phases, $f_c(\phi)$ in our toy model is a function with two wells; a broad one representing the fluid phase, and a narrower one at higher ϕ , representing the solid, as shown in Fig. 4. The ideal polymer's free energy density is

$$f_p = n_p \left[\ln \left(\frac{n_p}{\alpha(\phi)} \right) - 1 \right]$$

and the free volume fraction $\alpha(\phi)$ has the physically realistic values $\alpha(0) = 1$, $\alpha(1) = 0$, and becomes very small as $\phi \rightarrow 1$. The simple function $\alpha(\phi) = (1 - \phi)^7$ has the appropriate properties.

The resulting polymeric chemical potential is

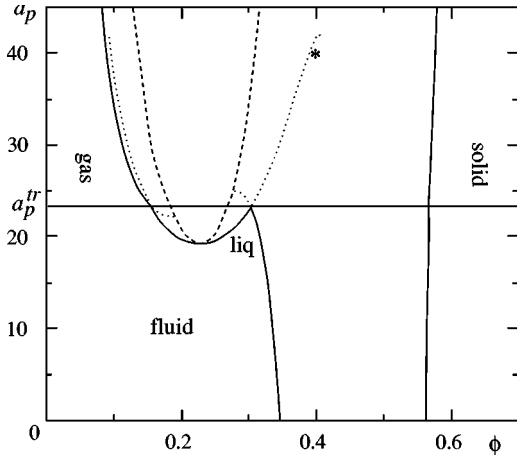


FIG. 5. The equilibrium phase diagram (solid lines) plus kinetic boundaries (dotted) and spinodal (dashed) in the plane of colloidal concentration ϕ and polymeric activity a_p , resulting from the toy semigrand potential, Eq. (3). Numerics were performed on an initial state at $*$.

$$\mu_p = \left(\frac{\partial f}{\partial n_p} \right)_\phi = \ln \frac{n_p}{\alpha(\phi)}.$$

Hence, we can make a Legendre transform to the semigrand potential density $\Omega(\phi) = f(\phi, n_p) - \mu_p n_p$, which is a function of colloidal concentration, parametrized by the polymeric chemical potential. In terms of the polymeric activity $a_p \equiv e^{\mu_p}$,

$$\Omega(\phi) = f_c(\phi) - a_p \alpha(\phi). \quad (3)$$

[See Fig. 4 for the form of $f_c(\phi)$.] For activities above the critical value $a_p^{\text{crit}} = 19.2$, $\Omega(\phi)$ has *three* minima; the effect of the polymer is to divide the fluid well of f_c into two, yielding separate gas and liquid phases.

We model the limit in which collective diffusion of polymer is much faster than that of colloid. Hence the gas of polymer is always fully equilibrated, so that a_p is uniform throughout the system. Nevertheless, as in the laboratory, polymer is conserved in our model. The mean density of polymer n_p is fixed throughout the evolution. For each instantaneous colloidal concentration profile $\phi(\mathbf{r})$, the total volume free to the polymer, $\int \alpha(\phi) d^3r$, is found. From this, a new polymeric activity a_p is calculated, and used to parametrize $\Omega(\phi)$.

B. The toy phase diagram

The phase diagram in Fig. 5, which includes metastable binodals delineating the predicted kinetic regimes, was produced by plotting the values of ϕ that are cotangential in Eq. (3), for a range of a_p . This phase diagram has the same topology as that of a colloid-polymer mixture with sufficiently large polymer. Triple coexistence is at $a_p \equiv a_p^{\text{tr}} = 23.2$, with phases of concentrations $\phi = 0.156, 0.304$, and 0.566 . In the absence of polymer (at $a_p = 0$), only two phases exist: fluid and solid (though we have not attempted to mimic the true hard-sphere binodal concentrations of 0.494

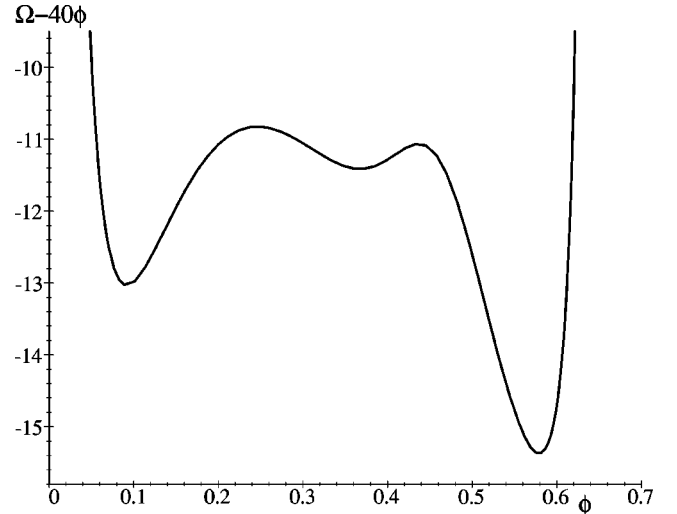


FIG. 6. The semigrand potential density $\Omega(\phi)$ at $a_p = 40$ in Fig. 5. An irrelevant linear part, 40ϕ , has been subtracted for clarity.

and 0.545). Gas-liquid, liquid-solid, and gas-solid cotangencies are shown dotted in Fig. 5 wherever they do not correspond to the lowest tangents on the $\Omega(\phi)$ curve (i.e., where they are metastable binodals). The gas and liquid branches that (locally) coexist with solid both end where they meet the gas-liquid spinodal (dashed). The corresponding solid branches cross at the triple line, and terminate shortly beyond it, though they are so close together that they appear as a single unbroken line in the figure. The metastable continuation of the gas-liquid binodal terminates at $a_p \approx 42$, where the liquid becomes unstable with respect to solidification, though this will not concern us.

C. Phase-ordering results

We model a situation in which a homogeneous metastable liquid is prepared at the point marked $*$ in Fig. 5 ($\phi = 0.4$, $n_p = 1.13$ in the arbitrary units of the toy model $\Rightarrow a_p^{\text{init}} = 40$), which is in kinetic region M (discussed in Secs. IV and IV B). For this composition, initially *above* the triple line, the *equilibrium* state is liquid-solid coexistence (*below* the triple line). The curve $\Omega(\phi)$, appropriate for a homogeneous system at $a_p = a_p^{\text{init}} = 40$, is shown in Fig. 6.

As our numerics contain no noise, the system will not evolve from an initially uniform concentration. At time zero, we introduce a small nucleus of a second phase: a sphere of gas at $\phi = 0.1$, centered on the origin, with radius 6. Concentration is plotted against radial distance in Fig. 7, where this initial state has a step profile, shown as a dashed line. Snapshots of the system's evolution at subsequent times are shown as solid lines. We see that the gas bubble rapidly collapses.⁸ Hence, as predicted, gas cannot nucleate first in region M .

⁸This is not a result of the bubble's radius being subcritical. Bubbles much larger than the characteristic interfacial width were also seen to collapse.

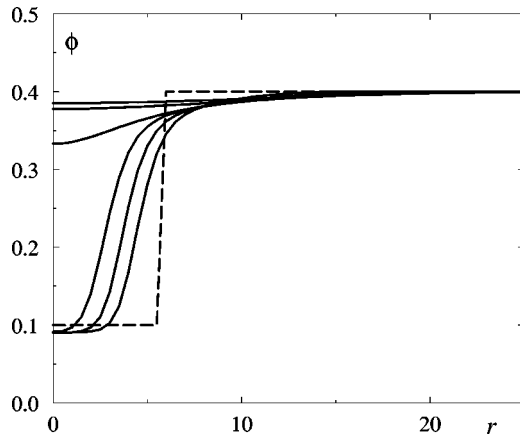


FIG. 7. The concentration profile $\phi(r)$ of a spherically symmetric gas nucleus immersed in a metastable liquid in region M . The initially sharp profile (dashed line) disperses over the subsequent times (full lines) $t=0.05, 0.1, 0.15, 0.2, 0.25, 0.3$.

In a second scenario, a spherical nucleus of solid ($\phi = 0.6$) of radius 3 (which is just supercritical) was introduced into the same metastable liquid. Snapshots of the evolution of its profile are shown in Fig. 8. The overall radius of the system is 300.

As shown in the inset to Fig. 8 the condensation nucleus very rapidly loses its artificially sharp boundary, acquiring instead a transitional zone, with width of order unity, from the concentration of the solid to that of the ambient liquid. The nucleus next loses its artificially high concentration $\phi = 0.6$, relaxing to a value around $\phi = 0.57$. Unlike the gas nucleus described above, this solid nucleus grows rapidly. In these early stages, there is an interface between the solid and the surrounding metastable liquid that cannot be described in terms of local quasiequilibrium between phases. In region M , no common tangent exists between the solid and liquid wells

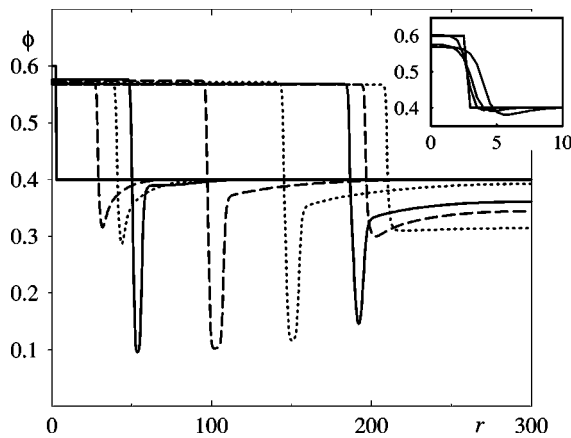


FIG. 8. The concentration profile $\phi(r)$ of a spherically symmetric solid nucleus immersed in a metastable liquid in region M . After an early stage of rapid growth, a shell of gas spontaneously forms around the solid, although there is no noise in the system. Eventually global equilibrium is attained, with no gas present. Snapshots are at $t=0$ (full line), 1.5 (dashed), 3 (dotted), 4.5 (full), 24 (dashed), 54 (dotted), 90 (full), 108 (dashed), 168 (dotted). Inset: Close up at $t=0, 10^{-4}, 10^{-3}, 10^{-2}$.

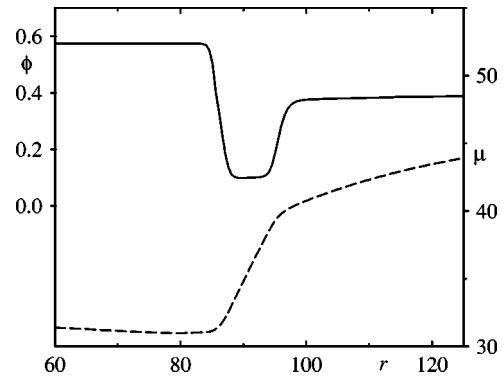


FIG. 9. Colloidal concentration ϕ (full line) and chemical potential μ (dashed line) in the neighborhood of the shell of the gas phase as a function of radial distance at time $t=18$. From left to right, the phases are solid, gas, liquid. The gradient of the chemical potential is highest in the gas phase.

of $\Omega(\phi)$, indicating that pressures and chemical potentials cannot be balanced across a solid-liquid interface. The interface observed early in the numerics is moving so fast that an equilibrium interface approximation is invalid. Nevertheless, the growth rate decreases with time, until such an approximation does hold. Accordingly, at $t \approx 3.7$, the solid nucleus acquires the predicted shell of gas, buffering it from the incompatible liquid. Though this gas appears suddenly and spontaneously, we recall that the algorithm is purely deterministic, containing no noise. For the sake of computational speed, it is tempting in the numerics to use a large grid spacing dr . Though the correct final equilibrium state was obtained using larger grids, the shell of gas only formed for $dr \approx 0.5$, which is several times smaller than interfacial widths and necessitates a very small time step for numerical stability.

When alone, a gas nucleus collapsed (Fig. 7), so the shell of gas in Fig. 8 relies, for its existence, on the presence of the solid. Despite this, the shell actually grows to a width much greater than the characteristic interfacial thickness. Its ability to do so is explained by Fig. 9 which is a close-up view of the concentration profile and the associated colloidal chemical potential profile in the neighborhood of the shell of gas phase at time $t=18$.

Material flows in response to the gradient of μ . We see in Fig. 9 that this gradient in the liquid phase (on the right of the picture) drives material towards the shell of gas, tending to fill it in, and thus destroy it. Nevertheless, the chemical potential gradient within the gas is high enough to drive a *larger* flux of material away from the liquid interface, making it recede. This material is deposited at the solid interface, where it is compacted, saving space. Despite the existence of a chemical potential gradient within the solid, driving material towards the gas cavity, the interface on the left of the gas advances more slowly than that on the right, so the gas phase grows. We believe this mechanism is not an artifact of the constancy of the mobility Γ . Whatever the form of $\Gamma(\phi)$, the system must organize itself so that diffusion through the gas shell out-competes the fluxes tending to collapse it.

As the solid nucleus grows, the metastable liquid is depleted in concentration, so free volume is made available for

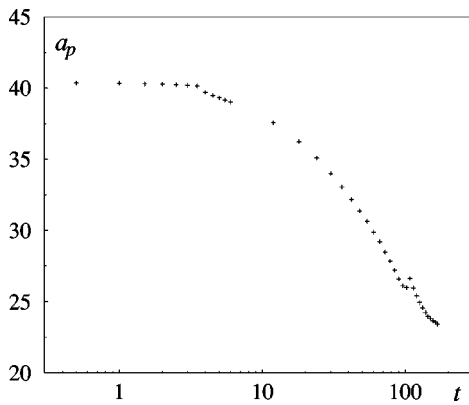


FIG. 10. Variation of polymeric activity throughout the phase-ordering process. Features at $t=3.7$ and $t=105$ betray the formation and subsequent disappearance of the gas shell. The final exponential relaxation to equilibrium appears as a linear tail in the logarithmic linear plot.

the finite amount of polymer. Hence polymeric activity a_p falls. For $a_p \approx 25$ (see Fig. 5) solid and liquid can exist in local equilibrium. Hence the gas shell eventually disappears from the system at $t \approx 105$. The time at which this occurs depends on the size of our model system or, in reality, on the distance between condensation nuclei. Finally, the system comes to equilibrium, with uniform regions of solid and liquid separated by a single interface.

Figure 10 shows the evolution of the uniform polymeric activity a_p with time t during the entire phase-ordering process. The general trend is downwards, since this corresponds to a lowering of the free energy of the ideal gas of polymer. However, this is not the only contribution to the free energy, and when the colloid finally removes its unfavorable gas phase from the system, it does so at the expense of polymeric entropy, so there is a small upturn in a_p at $t=105$.

It would be interesting to know how gravity would effect the unusual region M dynamics, in which gas forms despite being thermodynamically unfavorable. If the colloidal particles are denser than the solvent, gravity would tend to sepa-

rate some of the buoyant colloidal gas phase from the solid nuclei that it coats, and carry it to the top of the container. To attain thermodynamic equilibrium, the liquid and solid phases would subsequently have to rise, against gravity, to fill the gaseous void. It might be informative to model such a system.

VIII. SUMMARY AND CONCLUSION

We have shown that many distinct kinetic regimes can be charted within regions of equilibrium coexistence in the phase diagram, for a colloid-polymer mixture as for a wide variety of other systems. This we have done without reference to specific phenomenological equations of motion, since the second law of thermodynamics allows a great deal of information to be extracted from the nonconvex mean-field free energy as a function of conserved order parameters. It is difficult to assess whether the resulting phase-ordering pathways, given in Sec. IV C and mapped out in Fig. 3, explain all of the diverseness observed in colloid-polymer mixtures (reported in the preceding paper [16]), since the macroscopic experimental observations require some interpretation to infer the underlying microscopic processes. Certainly though, there appears to be sufficient richness in the physical results of our theory, and some of the observations at least (e.g., crystallites or gas phase being seen first [16]) are in quite clear agreement.

We expect that the concise notation of pathway diagrams will be useful in future studies, as they convey not only a sequence of possible events, but the causal relationships between them. It is hoped that the predicted novel mechanism of nucleation and growth, where a shell of one phase must intervene between another two, will be definitively observed in future experimental systems.

ACKNOWLEDGMENTS

We thank Michael Cates and Alastair Bruce for enlightening discussions. This work was supported by EPSRC Grant No. GR/K56025 and by the Royal Society of Edinburgh.

-
- [1] F. F. Abraham, Rep. Prog. Phys. **45**, 1113 (1982).
 - [2] J. D. Gunton and M. Droz, *Introduction to the Theory of Metastable and Unstable States*, Lecture Notes in Physics Vol. 183 (Springer, Berlin, 1983).
 - [3] J. D. Gunton, M. S. Miguel, and P. S. Sahni, in *Phase Transitions and Critical Phenomena*, edited by C. Domb and J. L. Lebowitz (Academic Press, London, 1983), Vol. 5, Chap. 3, p. 267.
 - [4] K. Binder, Rep. Prog. Phys. **50**, 783 (1987).
 - [5] H. Tanaka, Phys. Rev. Lett. **71**, 3158 (1993); **76**, 787 (1996).
 - [6] D. Sappelt and J. Jäckle, Europhys. Lett. **37**, 13 (1997).
 - [7] P. Rein ten Wolde and D. Frenkel, Science **277**, 1975 (1997).
 - [8] D. W. Oxtoby and P. R. Harrowell, J. Chem. Phys. **96**, 3834 (1992); V. Talanquer and D. W. Oxtoby, *ibid.* **100**, 5190 (1994).
 - [9] R. Wild and P. Harrowell, Phys. Rev. E **56**, 3265 (1997).
 - [10] M. P. Anisimov, P. K. Hopke, D. H. Rasmussen, S. D. Shandakov, and V. A. Pinaev, J. Chem. Phys. **109**, 1435 (1998).
 - [11] *Phase Transformations in Materials*, edited by R. W. Cahn, P. Haasen, and E. J. Kramer, Materials Science and Technology Vol. 5 (VCH, Weinheim, 1991).
 - [12] P. B. Warren, S. M. Ilett, and W. C. K. Poon, Phys. Rev. E **52**, 5205 (1995).
 - [13] S. M. Ilett, A. Orrock, W. C. K. Poon, and P. N. Pusey, Phys. Rev. E **51**, 1344 (1995).
 - [14] R. P. Sear, Phys. Rev. E **56**, 4463 (1997).
 - [15] C. Smits, B. Vandermost, J. K. G. Dhont, and H. N. W. Lekkerkerker, Adv. Colloid Interface Sci. **42**, 33 (1992); N. A. M. Verhaegh, J. S. van Duijneveldt, J. K. G. Dhont, and H. N. W. Lekkerkerker, Physica A **230**, 409 (1996).
 - [16] F. Renth, W. C. K. Poon, and R. M. L. Evans, preceding paper, Phys. Rev. E **64**, 031402 (2001).

- [17] J. W. Cahn, *J. Am. Ceram. Soc.* **52**, 118 (1969).
- [18] S. Asakura and F. Oosawa, *J. Chem. Phys.* **22**, 1255 (1954).
- [19] H. N. W. Lekkerkerker, W. C. K. Poon, P. N. Pusey, A. Stroobants, and P. B. Warren, *Europhys. Lett.* **20**, 559 (1992).
- [20] R. M. L. Evans, W. C. K. Poon, and M. E. Cates, *Europhys. Lett.* **38**, 595 (1997); R. M. L. Evans and M. E. Cates, *Phys. Rev. E* **56**, 5738 (1997); R. M. L. Evans and W. C. K. Poon, *ibid.* **56**, 5748 (1997).
- [21] H. B. Callen, *Thermodynamics and an Introduction to Thermostatistics*, 2nd ed. (John Wiley and Sons, Singapore, 1985).
- [22] O. Penrose, *J. Stat. Phys.* **78**, 267 (1995).
- [23] J. W. Cahn, *Trans. Metall. Soc. AIME* **242**, 166 (1968).
- [24] M. E. Fisher and S-Y. Zinn, *J. Phys. A* **31**, L629 (1998).
- [25] P. G. Debenedetti, *Metastable Liquids* (Princeton University Press, Princeton, 1996).
- [26] R. Roy, in *Symposium on Nucleation and Crystallization of Glass*, edited by M. Reser, G. Smith, and H. Insley (American Ceramic Society, Columbus, OH, 1962).
- [27] W. van Meegen, S. M. Underwood, and I. Snook, *J. Chem. Phys.* **85**, 4065 (1986).
- [28] M. D. Haw, W. C. K. Poon, P. N. Pusey, P. Hebraud, and F. Lequeux, *Phys. Rev. E* **58**, 4673 (1998).
- [29] R. M. L. Evans, M. E. Cates, and P. Sollich, *Eur. Phys. J. B* **10**, 705 (1999).
- [30] W. C. K. Poon, A. D. Pirie, and P. N. Pusey, *Faraday Discuss.* **101**, 65 (1995); W. C. K. Poon, L. Starrs, S. P. Meeker, A. Moussaïd, R. M. L. Evans, P. N. Pusey, and M. M. Robins, *ibid.* **112**, 143 (1999); M. C. Grant and W. B. Russel, *Phys. Rev. E* **47**, 2606 (1993); J. Bergenholtz and M. Fuchs, *ibid.* **59**, 5706 (1999).
- [31] W. C. K. Poon, *Phys. Rev. E* **55**, 3762 (1997).
- [32] K. G. Soga, J. R. Melrose, and R. C. Ball, *J. Chem. Phys.* **110**, 2280 (1999).
- [33] J. Buitenhuis, L. N. Donselaar, P. A. Buining, A. Stroobants, and H. N. W. Lekkerkerker, *J. Chem. Phys.* **175**, 46 (1995); M. P. B. van Bruggen, F. M. van der Kooij, and H. N. W. Lekkerkerker, *J. Phys.: Condens. Matter* **8**, 9451 (1996).
- [34] P. M. Chaikin and T. C. Lubensky, *Principles of Condensed Matter Physics* (Cambridge University Press, Cambridge, UK, 1995).
- [35] J. W. Cahn and J. E. Hilliard, *J. Chem. Phys.* **28**, 258 (1958).